2015

Visualization of 4D Q2PSK and CE Q2PSK in Ideal Bandlimited Channels

Milton I. Quinteros
University of New Orleans

Edit J. Kaminsky
University of New Orleans, ejbourge@uno.edu

Kenneth V. Cartwright
College of The Bahamas

Recommended Citation

Quinteros, M., E.J. Kaminsky, and K.V. Cartwright, “Visualization of 4D Q2PSK and CE Q2PSK in ideal bandlimited channels,” IEEE WCNC 2015, (New Orleans, March 2015), pp. 499-504.

Visualization of 4D Q^2PSK and CEQ^{2}PSK in Ideal Bandlimited Channels

Milton I. Quinteros
Dept. of Electrical Engineering
EN 616A Lakefront Campus
University of New Orleans
New Orleans, LA 70148, U.S.A.
Email: mquinter@uno.edu

Edit J. Kaminsky
Dept. of Electrical Engineering
EN 846 Lakefront Campus
University of New Orleans
New Orleans, LA 70148, U.S.A.
Email: ejbourge@uno.edu

Kenneth V. Cartwright
School of Mathematics, Physics and Technology
College of The Bahamas
P.O. Box N4912
Nassau, Bahamas
Email: kvc@batelnet.bs

***Abstract*—This paper presents new visualization techniques for 4D Quadrature-Quadrature Phase Shift Keying (Q^2PSK), Saha's Constant Envelope (CE) Q^2PSK, and Cartwright's CEQ^{2}PSK in ideal bandlimited channels. The signal diagrams analyzed are: time-signal eye patterns for 4D passband signals, 2D complex trajectory diagrams of baseband signals, and time-signal eye patterns for the 1D outputs of the baseband matched filter. These methods may be applied to other multidimensional modulation systems to obtain insight into the effects of noise, interference, and channel filtering.**

***Index Terms*—Q^2PSK, CEQ^{2}PSK, bandlimited channel, constant envelope, signal trajectory diagram, eye diagram, visualization.**

I. Introduction

Shannon proposed geometrical representations of signals in [1], where he discussed the association of information signals with Euclidean spaces, resulting in an understanding of the relationship between visual indicators and the performance of digital communications systems. Since then, effort has been devoted by other researchers to connect the multidimensional geometric representations to communication systems' waveforms and to visually represent these high-dimensional constellations in lower-dimensional spaces.

In this paper, we discuss new visualization methods for 4D Q^2PSK systems; in particular, we analyze Q^2PSK [2, 3] and CEQ^{2}PSK [4–6] systems with no channel bandlimitation as well as with ideal channel filters of baseband bandwidth $\frac{0.6}{T}$ and $\frac{1}{T}$, where $2T$ is the 4D symbol interval.

In [7, Fig.1], Saha and El-Ghandour present a 4D Q^2PSK signal space diagram where the four dimensions are decoupled into two 2D sub-spaces associated with the hal-cosine and the half-sine pulses; the diagram shows the decoupled phase points of Q^2PSK around each pulse axis. Similarly, in [8, Fig. 2.5] Cilliers describes a visualization of Q^2PSK where the signal constellations points are plotted around a frequency axis. Cilliers also discusses two graphical representations of the projection of the 4D Q^2PSK hypercube onto 3D cubes ([8, Figs. 2.10, 2.11]). These latter four representations aid in visualizing 4D systems, but provide no insight or information about the transmitted or received signals; our visualization work, on the other hand, aids the understanding of the deleterious effects of noise and interference. Drakul and Biglieri [9, Figs. 2, 3] portray all pulses vs. time for one signaling interval and also eye patterns (see [9, Figs. 5, 7]) for an 8D Constant Envelope modulation Scheme (8D-CEMS). Malan shows in [10, Fig. 6.2] a complex 2D baseband envelope diagram of a 4D Direct Sequence Spread Spectrum (DSSS) signal to portray amplitude and phase distortions caused by a bandlimited channel.

Our first visualization method, the time-signal eye pattern, consists of portraying the set of all possible 4D passband filtered signals versus time; we choose to display times from $-T$ to T, to show the entire 4D signaling interval, using the minimum carrier frequency. The second method is a 2D complex trajectory diagram in which the baseband in-phase and in-quadrature signals are plotted versus each other with time as a parameter. The third method represents the output of the matched filter (before the sample and hold operation) for each of the 4 components, versus time, for times between 0 and $2T$, to show the decision time in the middle.

The rest of this paper is organized as follows: The first section is a brief review of Q^2PSK and Saha's and Cartwright's CEQ^{2}PSK. Next, in Section III, we present the visualization methods used. Results are presented and discussed in Section IV. Concluding remarks and proposals for future work are given in Section V, followed by cited references.

II. Review of 4D Q^2PSK

In this section, we summarize Q^2PSK, Saha's CEQ^{2}PSK, and Cartwright's CEQ^{2}PSK.

A. *Q^2PSK*

Q^2PSK [2] is a 4D modulation scheme defined by:

$$\begin{aligned} S(t) = a_1 p_1(t)\cos(\omega_c t) + a_2 p_2(t)\cos(\omega_c t) + \\ + a_3 p_1(t)\sin(\omega_c t) + a_4 p_2(t)\sin(\omega_c t), \end{aligned} \tag{1}$$

where $\{a_i\}$, $i = 1, \ldots, 4$, are ± 1, the half-cosine and half-sine pulses, $p_1(t)$ and $p_2(t)$, are given by (2), the carrier angular frequency, ω_c, is $n\pi/2T$, with n $\geq$2, and T is the duration of 2 bits.

$$p_j(t) = \cos\left(\frac{\pi t}{2T} - \frac{(j-1)\pi}{2}\right), \ \ |t| \leq T, \ \ j = 1, 2. \tag{2}$$

Eq. (1) may also be represented as

$$S(t) = A(t)\cos\left(\omega_c t + \theta(t)\right), \tag{3}$$

where the amplitude and phase are given, respectively, by (4) and (5):

$$A(t) = \left(2 + (a_1 a_2 + a_3 a_4)\sin(\pi t/T)\right)^{1/2}, \tag{4}$$

$$\theta(t) = \tan^{-1}\left(\frac{a_3\cos(\pi t/2T) + a_4\sin(\pi t/2T)}{a_1\cos(\pi t/2T) + a_2\sin(\pi t/2T)}\right). \tag{5}$$

Equivalently, we could use a baseband model for (1) in which the k^{th} transmitted Q^{2}PSK signal is:

$$\begin{aligned} S_k(t) = &\, a_{1,k}p_1(t-2kT) + a_{2,k}p_2(t-2kT) + \\ &-j[a_{3,k}p_1(t-2kT) + a_{4,k}p_2(t-2kT)]. \end{aligned} \tag{6}$$

The real part of (6) is the in-phase component, I, and the imaginary part corresponds to the quadrature-phase, Q. There are 16 4D symbols that form this non-constant envelope Q^{2}PSK signal set. Saha's Q^{2}PSK points are listed on the left side of Table I; we have separated the eight points that have constant envelope (listed in the bottom) from the other eight. The fourth component of the top eight Q^{2}PSK vectors is $a_4 = a_1a_2/a_3$ while for the bottom eight, this component is $a_4 = -a_1a_2/a_3$. For the top 8 points the phase is piecewise-constant with values $\theta(t) \in \{\pm 45°, \pm 135°\}$; the bottom 8 points have phase values that increase or decrease piece-wise linearly.

TABLE I
4D Q^{2}PSK POINTS.

	Saha's				Cartwright's				
	a_1	a_2	a_3	a_4	a_1	a_2	a_3	a_4	
Magnitude: variable Phase: $\pm 45°$ $\pm 135°$	-1	-1	-1	-1	0	$-\sqrt{2}$	0	$-\sqrt{2}$	Magnitude: $\sqrt{2}$ Phase: $\pm 45°$ $\pm 135°$
	-1	-1	1	1	0	$-\sqrt{2}$	0	$\sqrt{2}$	
	-1	1	-1	1	$-\sqrt{2}$	0	$-\sqrt{2}$	0	
	-1	1	1	-1	$-\sqrt{2}$	0	$\sqrt{2}$	0	
	1	-1	-1	1	$\sqrt{2}$	0	$-\sqrt{2}$	0	
	1	-1	1	-1	$\sqrt{2}$	0	$\sqrt{2}$	0	
	1	1	-1	-1	0	$\sqrt{2}$	0	$-\sqrt{2}$	
	1	1	1	1	0	$\sqrt{2}$	0	$\sqrt{2}$	
Magnitude: $\sqrt{2}$ Phase: piecewise linear	-1	-1	-1	1	0	$-\sqrt{2}$	$-\sqrt{2}$	0	Magnitude: $\sqrt{2}$ Phase: piecewise linear
	-1	-1	1	-1	0	$-\sqrt{2}$	$\sqrt{2}$	0	
	-1	1	-1	-1	$-\sqrt{2}$	0	0	$-\sqrt{2}$	
	1	-1	-1	-1	$\sqrt{2}$	0	0	$-\sqrt{2}$	
	1	1	1	-1	0	$\sqrt{2}$	$\sqrt{2}$	0	
	1	1	-1	1	0	$\sqrt{2}$	$-\sqrt{2}$	0	
	1	-1	1	1	$\sqrt{2}$	0	0	$\sqrt{2}$	
	-1	1	1	1	$-\sqrt{2}$	0	0	$\sqrt{2}$	

B. *CEQ^{2}PSK*

In [4] and [5], respectively, two 4D constant envelope constellations were introduced: Saha's CEQ^{2}PSK and Cartwright's CEQ^{2}PSK. Constant envelope is obtained at the expense of a reduction in the transmission rate, by ensuring that $a_4 = -a_1a_2/a_3$. Each set has eight 4D symbols and makes $A(t)$ in (4) a constant value equal to $\sqrt{2}$ [5]. The original two CEQ^{2}PSK constelations are those listed on the bottom half of Table I as having magnitude $\sqrt{2}$. Notice that there are two constellations of Cartwright-type symbols: Cartwright's original constellation presented in [5], listed on the bottom right corner of Table I, and another we are presenting here for the first time, listed on the top right corner of this same table. This constellation also has constant envelope with $A(t) = \sqrt{2}$, for all t, but has piece-wise constant phase, while Cartwright's original CEQ^{2}PSK constellation has piecewise-linear phase.

III. VISUALIZATION METHODS

In this Section we explain our three graphical representations used to visualize the signals of interest. Our work was motivated by the lack of insight into the effects of noise and interference provided by previous multidimensional signal diagrams. The methods described in this Section allow us to better understand the effects of filtering on the 4D transmitted signals in passband, the in-phase and quadrature 2D components in baseband, and the the individual 1D components at the output of the matched filter.

A. *Time-signal eye patterns for 4D passband signals*

The time-signal eye pattern is obtained by plotting (1) or (3) with $\omega_c = \pi/T$, or the channel-filtered version of these, for all combinations of possible 4D signals, versus time. Any other allowed carrier frequency may be chosen, but no further insight about the modulated signals is obtained by doing this. These signals are presented on the same graph over a period of $2T$ –the length of one 4D symbol– showing a complete 4D signaling interval from $-T$ to T. Notice that (1) and (3) depend on $[a_1\, a_2\, a_3\, a_4]$ which for CEQ^{2}PSK is a subset of the possible Q^{2}PSK vectors (see Table I). By using this method, the amplitude and phase of the passband signal are shown graphically for all times.

B. *2D complex trajectory diagrams for 4D baseband signals*

With this method we look at the baseband version of the 4D modulated signal in the complex plane by showing parametric plots of the trajectories of the in-phase component versus the quadrature-phase component of the signal in (6), or a filtered version of it as shown in (6) of [11]. Effectively, the 2D complex trajectories are polar diagrams of the magnitude in (4) and the phase in (5) –or, again, filtered versions of these– with time as a parameter. The trajectory diagram clearly shows distortions caused by the ISI created by the bandlimited channel.

C. *Time-signal eye pattern for the 1D outputs of the baseband matched filter*

The baseband receiver, consisting of a bank of two pairs of matched filters, separates the real parts (in-phase) from the imaginary parts (quadrature-phase) and also the half-cosine pulses from the half-sine pulses. We also use time-signal eye diagrams to show each component of the baseband signals at the output of the matched filter. All possible signals for each component are superimposed, for a single signaling interval. The four signals at the output of the matched filter, if the channel has infinite bandwidth, are:

$$\begin{aligned} y_k(t) &= a_k p_1(t) * h_1(t) + a_{k+1} p_2(t) * h_1(t) \\ &= a_k y'_{11}(t-T) + a_{k+1} y'_{12}(t-T), \end{aligned} \tag{7a}$$

$$\begin{aligned} y_m(t) &= a_{m-1} p_1(t) * h_2(t) + a_m p_2(t) * h_2(t) \\ &= -a_{m-1} y'_{12}(t-T) - a_m y'_{22}(t-T), \end{aligned} \tag{7b}$$

for $k = 1, 3$, $m = 2, 4$, and y'_{ij} given in (8). The matched-filter impulse responses are $h_1(t) = p_1(T-t)$ and $h_2(t) = p_2(T-t)$, with $p_j(t)$ given in (2).

$$\begin{aligned} y'_{ij}(t) = \frac{(-1)}{2}^{(i-1)(j-1)} &\cos\left[\frac{\pi}{2}\left(\frac{t}{T} - |i-j|\right)\right](2T - |t|) + \\ +\frac{T}{\pi}\sin\left(\frac{\pi|t|}{2T}\right)&|3-i-j|, \quad |t| \le 2T, \end{aligned} \tag{8}$$

for $i, j = 1, 2$.

The open parts of the time-signal eye patterns occur around decision time T. For Saha's signals there is a single eye, while for Cartwrights' there are two, as three levels are possible. The horizontal eye opening relates to the phase and shows the sensitivity to sampling instant shifts (i.e., synchronization). In addition, the amplitude distortion at the sampling time –which relates directly to the modified geometry of the 4D signals with ISI– also becomes obvious.

IV. Visualization Results

In this section we present and discuss the results of our visualization analysis of Q^{2}PSK signals.

A. Time-signal eye patterns for 4D passband Q^{2}PSK

Figure 1 portrays the time-signal eye patterns for the three 4D passband systems of interest. The columns correspond, respectively, to Q^{2}PSK, Saha's CEQ^{2}PSK, and Cartwright's original CEQ^{2}PSK. The rows represent the bandwidth limitation: for the plots on the top row there is no channel filter, while the second and third rows have channels bandlimited to $\frac{1}{T}$ and $\frac{0.6}{T}$, respectively, where 2T is the 4D symbol interval. We see in a) the 16 traces of all possible Q^{2}PSK 4D symbols, with symbol transitions occurring at times 0 and $2T$ and possible phase changes of 0, $\pm 90°$ and $\pm 180°$, as stated in [2]. For the filtered Q^{2}PSK signals there are 4096 traces on the 4D passband time-signal eye patterns because we assume that one past, one present, and one future symbol affect the current symbol, and each one of these has 16 possible values. If one compares a) to b) and c), it becomes clear that amplitude distortion is introduced by the bandlimited channels. The possible values of the signals with ISI are no longer just ± 1 at $-T$, 0, and T, and many new phase changes occur.

Results for Saha's and Cartwright's original CEQ^{2}PSK are portrayed on the second and third columns of Fig. 1, respectively. Because d) and g) show the signals without bandlimitation, there are 8 traces displayed. The symbol transitions again occur at time 0 and $2T$ and we also have possible abrupt changes in phase at those times. The possible phase shifts are still 0, $\pm 90°$ and $\pm 180°$, as they were for Q^{2}PSK. Because e), f), h) and i) depict signals with ISI, there are 512 traces when the memory is truncated to three symbols. When Cartwright's original CEQ^{2}PSK is used, the possible values of the unfiltered 4D signal at time T are 0 and $\pm\sqrt{2}$; clearly, the 4D Euclidean distances at that time are equal for Saha's and Cartwright's constellations, but at time T the minimum distance has been reduced from 2 to $\sqrt{2}$ while the maximum distance has been increased from 2 to $2\sqrt{2}$. Again, multiple new phase angles are now present.

B. 2D complex trajectory diagrams for Q^{2}PSK signals

Figure 2 shows the complex trajectory diagrams for the systems of interest. Notice that both the amplitude and phase information of the 4D signals are shown with time as a parameter, by plotting the in-phase component vs. the quadrature-phase. Because time is not shown, the abrupt phase changes of the unfiltered signals are only easily seen in Fig. 2 a), i.e., for Q^{2}PSK. On the other hand, the constant envelope is obvious for the CEQ^{2}PSK unfiltered systems shown in d) and g). It is also clear that the complex trajectory diagram for Cartwright's CEQ^{2}PSK is a $45°$ rotation of the diagram for Saha's CEQ^{2}PSK; as noted in [5], Cartwright's constellation is obtained by performing two 2D rotations of $45°$ on Saha's 4D points. Using this visualization method we readily see that the ISI-distorted CEQ^{2}PSK signals are no longer of constant envelope and may even be zero at certain instants.

C. Time-signal eye patterns of the 1D baseband matched filter outputs for Q^{2}PSK

The time-signal eye pattern at the output of the matched filter helps visualize the signal geometry because the shifted coefficients $\hat{c}_i$ that arise from the signal with ISI become clear at time T, the sampling time of the sample-and-hold device at the receiver. The possible values of (7a) and (7b) are plotted on the first row of Fig. 3; a) and d) correspond to Q^{2}PSK and Saha's CEQ^{2}PSK, while g) and j) are for Cartwright's original CEQ^{2}PSK. We computed the values of these coefficients using (7) from [11] and list them in Table II for Cartwright's original constellation at the two bandwidths of interest to us, and on Table I of [11] for Saha's constellation. These coefficients are the possible values at $t = T$ when the ISI is truncated to three signaling intervals. The numbers listed in the last column, N, indicate the number of occurrences of each coefficient in the new geometry; there are a total of 512 signal points.

The vertical (amplitude) and horizontal (time) eye openings at the output of the matched filter are listed in Table III for the systems discussed in this paper, both filtered and unfiltered; we also show the percentage decrease in the length of the eye opening in each direction, as it is this reduction in the size of the eye that helps us visualize the likelihood of detection errors. We define the vertical aperture, VA, as the minimum 1D distance between possible amplitudes at sampling time T. The horizontal aperture, HA, for unfiltered signals is defined as the length of time between signal crossings (excluding those with 0-amplitude crossing). When the signals are filtered, we measure the corresponding minimum distance. Both VA and HA are indicated with arrows on Fig. 3. The amplitude

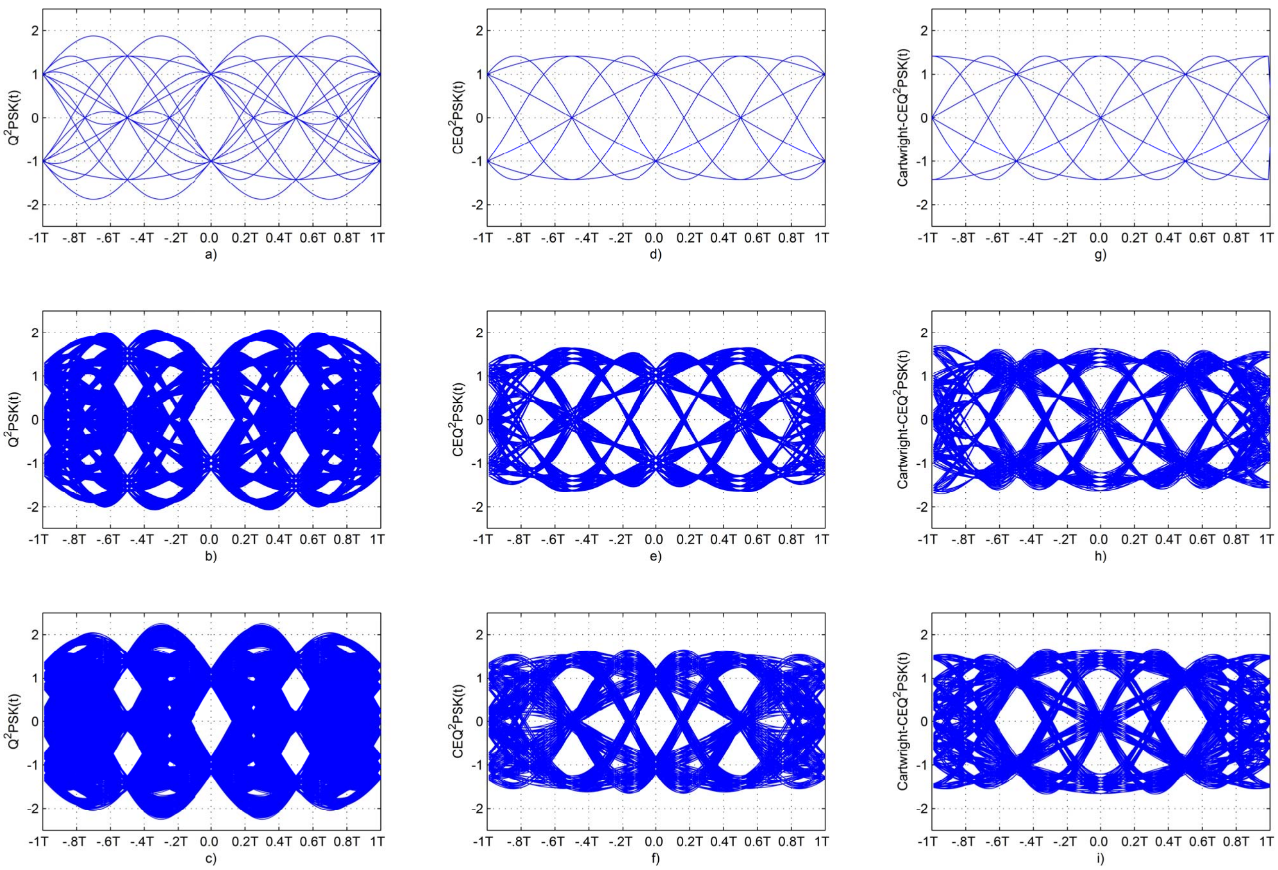

Fig. 1. Time-signal eye patterns for 4D passband signals. Q^{2}PSK: a) unfiltered, b) filtered at B_1, c) filtered at B_2. Saha's CEQ^{2}PSK: d) unfiltered, e) filtered at B_1, f) filtered at B_2. Cartwright's CEQ^{2}PSK: g) unfiltered, h) filtered at B_1, i) filtered at B_2. $B_1 = 1/T, B_2 = 0.6/T$.

TABLE II
MAGNITUDE OF THE COEFFICIENTS FOR TWO CHANNEL BANDWIDTHS FOR CARTWRIGHT'S CEQ^{2}PSK.

$B_1 = \frac{1}{T}$		$B_2 = \frac{0.6}{T}$		
$\hat{c}_1$ or $\hat{c}_3$	$\hat{c}_2$ or $\hat{c}_4$	$\hat{c}_1$ or $\hat{c}_3$	$\hat{c}_2$ or $\hat{c}_4$	N
0	0	0	0	64
0.001915	0.007582	0.005313	0.016256	32
0.003751	0.073442	0.005448	0.085718	64
0.005666	0.081023	0.010759	0.101973	64
0.007582	0.154465	0.016207	0.187691	32
1.403177	1.107992	1.380991	0.988777	16
1.405092	1.181434	1.386439	1.074494	32
1.407008	1.189016	1.391751	1.160212	16
1.408843	1.254875	1.391887	1.090750	32
1.410759	1.262457	1.397199	1.176467	64
1.414509	1.270039	1.402510	1.192723	16
1.412674	1.335899	1.402646	1.262185	32
1.416425	1.343481	1.407958	1.278441	32
1.418340	1.416922	1.413406	1.364158	16

distortions that correspond to the cosine pulses is always small, while it is considerably larger for the sine pulses. The sine components are also more prone to timing errors, as seen by the eye narrowing in the horizontal direction. The probability of error performance in Additive White Gaussian Noise (AWGN) channels depends on the minimum Euclidean distance between 4D points. One must remember that for Cartwright's constellation, if the amplitude of one half-cosine pulse is not 0, the other one is and that the same applies to the half-sine pulses. This means that, without error correction, the apertures may be minimum in each of the four components of Saha's constellation, while this is not possible in Cartwright's.

V. CONCLUSIONS AND FURTHER WORK

We have presented visualization aids for 4D Q^{2}PSK, both constant and non-constant envelope, as well as filtered and unfiltered. This is an effort to gain insight into the behaviour of these signals in bandlimited channels. The diagrams shown help to visualize the causes of the degradation in probability of error performance when the channel is bandlimited and therefore ISI is introduced.

Future work will include a thorough evaluation of the performance of both of Cartwright's CEQ^{2}PSK constellations in bandlimited channels and a comparison to Saha's. More

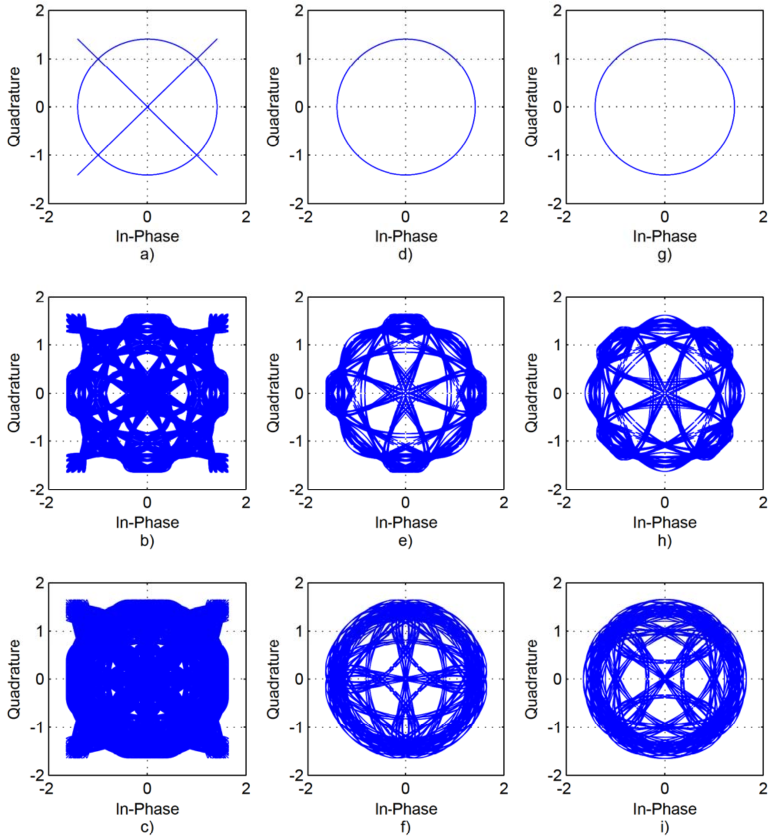

Fig. 2. 2D complex trajectory diagrams. Q^2PSK: a) unfiltered, b) filtered at B_1, c) filtered at B_2. Saha's CEQ^2PSK: d) unfiltered, e) filtered at B_1, f) filtered at B_2. Cartwright's CEQ^2PSK: g) unfiltered, h) filtered at B_1, i) filtered at B_2. $B_1 = 1/T, B_2 = 0.6/T$.

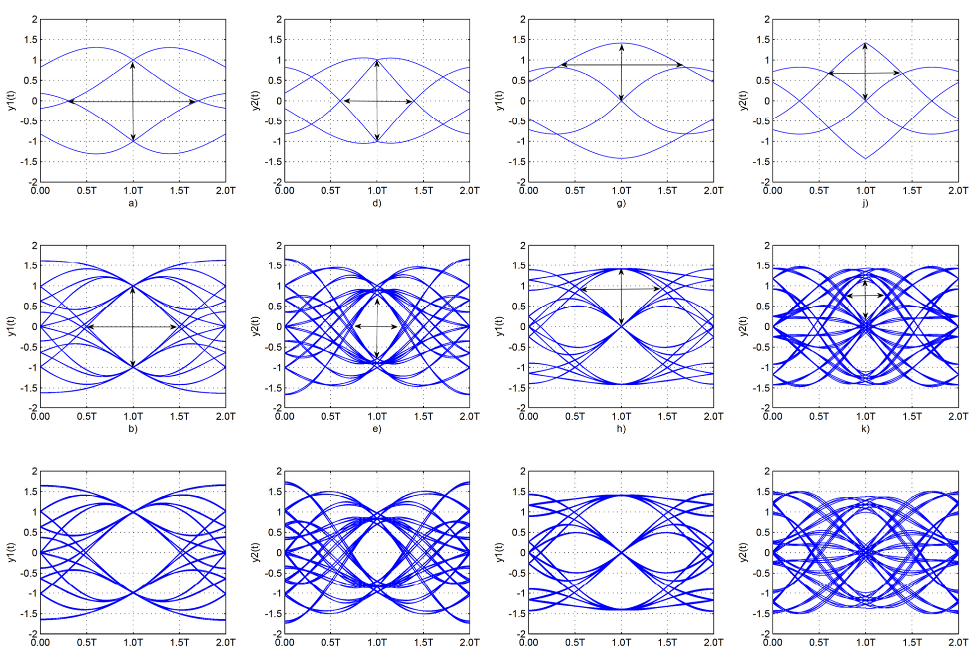

Fig. 3. Time-signal eye patterns of the 1D output of the baseband matched filter. Q^2PSK and Saha's CEQ^2PSK: a) unfiltered a_1 and a_3, b) a_1 and a_3 filtered at B_1, c) a_1 and a_3 filtered at B_2, d) unfiltered a_2 and a_4, e) a_2 and a_4 filtered at B_1, f) a_2 and a_4 filtered at B_2. Cartwright's CEQ^2PSK: g) unfiltered a_1 and a_3, h) a_1 and a_3 filtered at B_1, i) a_1 and a_3 filtered at B_2, j) unfiltered a_2 and a_4, k) a_2 and a_4 filtered at B_1, l) a_2 and a_4 filtered at B_2. $B_1 = 1/T,\ B_2 = 0.6/T$.

TABLE III
AMPLITUDE AND TIME APERTURES AT MATCHED FILTER OUTPUT.

			$B_o = \infty$	$B_1 = \frac{1}{T}$		$B_2 = \frac{0.6}{T}$	
			Aperture	Aperture	% decrease	Aperture	% decrease
Saha's Q^2PSK & CEQ^2PSK	$y_1(t)$	VA	2.00	1.98	1.00	1.95	2.50
		HA	1.4T	1.0T	28.57	1.0T	28.57
	$y_2(t)$	VA	2.00	1.56	22.00	1.37	31.50
		HA	0.8T	0.6T	25.00	0.6T	25.00
Cartwright's CEQ^2PSK	$y_1(t)$	VA	$\sqrt{2}$	1.40	1.00	1.36	3.83
		HA	1.4T	0.8T	42.85	0.8T	42.85
	$y_2(t)$	VA	$\sqrt{2}$	0.95	32.83	0.80	43.43
		HA	0.8T	0.4T	50.00	0.4T	50.00

realistic models of bandlimited and fading channels will be used.

We will also apply a continuous Morlet wavelet transform to Q^2PSK systems, which shall be used to visualize, simultaneously, the time-frequency behavior of the bandlimited signals and used to develop a wavelet-based receiver that estimates the phase-shift, ISI, and noise-type of actual channels. The performance of such receiver is expected to be superior to the standard matched filter –optimum in AWGN– when other deleterious effects are introduced by the channel, particularly in the presence of impulsive and colored noise.

REFERENCES

[1] C. E. Shannon, "Communication in the presence of noise," *Proc. of the IRE*, vol. 37, no. 1, pp. 10–21, 1949.

[2] D. Saha and T. G. Birdsall, "Quadrature-quadrature phase shift keying," *IEEE Trans. Commun.*, vol. 37, no. 5, pp. 437–448, May 1989.

[3] J. S. Han and M. J. Kim, "Offset quadrature-quadrature phase shift keying with half-sine pulse shaping," in *Proc. ICTC 2013, Internat. Convergence Tech. Conf.*, 2013, pp. 931–935.

[4] D. Saha, "Quadrature-quadrature phase shift keying with constant envelope," US Patent 4,730,344, Mar. 8, 1988.

[5] M. I. Quinteros, E. J. Kaminsky, K. V. Cartwright, and R. U. Gallegos, "A novel expanded 16-dimensional constant envelope Q^2PSK constellation," in *Proc. IEEE TechCon 2008, Region 5 Conference*, Kansas City, MO, Apr. 17-20 2008, pp. 1–6.

[6] K. Priya and M. Tamilarasi, "A trellis-coded modulation scheme with 32-dimensional constant envelope Q^2PSK constellation," in *Proc. ICCSP 2013, Internat. Conf. Commun. Signal Proc.*, 2013, pp. 821–825.

[7] D. Saha and O. El-Ghandour, "Differentially coherent quadrature-quadrature phase shift keying (Q^2PSK)," in *Conf. Record IEEE MILCOM 1990, Military Commun. Conf.*, vol. 2, Sept. 1990, pp. 585–589.

[8] J. E. Cilliers, "Multi-dimensional lattice equaliser for Q^2PSK," Master's thesis, University of Pretoria, 2002.

[9] S. Drakul and E. Biglieri, "A class of constant envelope multidimensional modulation schemes for non-linearly amplified channels," in *Singapore ICCS '94. Conference Proceedings.*, vol. 1, Nov. 1994, pp. 114–118.

[10] E. Malan, "Multi-dimensional direct-sequence spread spectrum multiple-access communication with adaptive channel coding," Master's thesis, University of Pretoria, 2006.

[11] M. Quinteros, E. J. Kaminsky, and K. V. Cartwright, "Performance and spectral analysis of Q^2PSK and CEQ^2PSK systems in ideal bandlimited channels," in *Proc. IEEE GLOBECOM 2014*, Dec. 2014, pp. 3621–3626.